*Article*

# Spatiotemporal Analysis of Fire Foci and Environmental Degradation in the Biomes of Northeastern Brazil

José Francisco de Oliveira-Júnior [1,*], Munawar Shah [2,*], Ayesha Abbas [3], Washington Luiz Félix Correia Filho [4], Carlos Antonio da Silva Junior [5], Dimas de Barros Santiago [6], Paulo Eduardo Teodoro [7], David Mendes [8], Amaury de Souza [9], Elinor Aviv-Sharon [10], Vagner Reis Silveira [11], Luiz Claudio Gomes Pimentel [12], Elania Barros da Silva [13], Mohd Anul Haq [14,*], Ilyas Khan [15], Abdullah Mohamed [16] and El-Awady Attia [17,18]

1    Laboratório de Meteorologia Aplicada e Meio Ambiente (LAMMA), Insstituto de Ciências Atmosféricas (ICAT), Universidade Federal do Alagoas (UFAL), Maceió 57072-260, Brazil
2    GNSS and Space Education Research Lab, Department of Space Science, National Center of GIS and Space Applications, Institute of Space Technology, Islamabad 44000, Pakistan
3    Department of Petroleum Engineering, NED University of Engineering and Technology, Karachi 75270, Pakistan; ayeshaabbas@cloud.neduet.edu.pk
4    Institute of Mathematics, Statistics and Physics, Federal University of Rio Grande, Rio Grande 96203-900, Brazil; washington.correia@furg.br
5    Geotechonology Applied in Agriculture and Forest (GAAF), State University of Mato Grosso (UNEMAT), Sinop 78555-000, Brazil; carlosjr@unemat.br
6    Postgraduate Program in Meteorology, Unidade Acadêmica de Ciências Atmosféricas (UACA), Federal University of Campina Grande (UFCG), Campina Grande 58429-140, Brazil; dimas.barros@estudante.ufcg.edu.br
7    Department of Agronomy, Federal University of Mato Grosso do Sul (UFMS), Chapadão do Sul 79560-000, Brazil; paulo.teodoro@ufms.br
8    Post-Graduate Program in Aerospace Engineering (PPGEA), Federal University of Rio Grande do Norte (UFRN), Campus Universitário Lagoa Nova, Natal 59056-000, Brazil; david.mendes@ufrn.br
9    Physics Institute, Federal University of Mato Grosso do Sul (UFRN), C.P. 549, Campo Grande 79070-900, Brazil; amaury.souza@ufms.br
10   Department of Plant and Environmental Sciences, Weizmann Institute of Science, Rehovot 7610001, Israel; elinor.aviv@weizmann.ac.il
11   Departamento PROEAD, Centro Universitário de Goiás, Goiânia 74423-115, Brazil; vagner.silveira@unigoias.com.br
12   Department of Meteorology, Institute of Geosciences, Federal University of Rio de Janeiro, Av. Athos da Silveira Ramos, 274 Cidade Universitária—Ilha do Fundão, Rio de Janeiro 21941-916, Brazil; luizpimentel@igeo.ufrj.br
13   Pós-Graduação em Engenharia de Biossistemas (PGEB), Universidade Federal Fluminense (UFF), Niterói 24210-240, Brazil; barroselania@id.uff.br
14   Department of Computer Science, College of Computer and Information Sciences, Majmaah University, Al-Majmaah 11952, Saudi Arabia
15   Department of Electrical Engineering, Department of Mathematics, College of Science Al-Zulfi, Majmaah University, Al-Majmaah 11952, Saudi Arabia; i.said@mu.edu.sa
16   University Research Centre, Future University in Egypt, New Cairo 11745, Egypt; mohamed.a@fue.edu.eg
17   Department of Industrial Engineering, College of Engineering, Prince Sattam Bin Abdulaziz University, Al-Kharj 16273, Saudi Arabia; e.attia@psau.edu.sa
18   Mechanical Engineering Department, Faculty of Engineering (Shoubra), Benha University, Cairo 11511, Egypt
*    Correspondence: jose.junior@icat.ufal.br (J.F.d.O.-J.); munawar.shah@mail.ist.edu.pk (M.S.); m.anul@mu.edu.sa (M.A.H.)

**Abstract:** Forest fires destroy productive land throughout the world. In Brazil, mainly the Northeast of Brazil (NEB) is strongly affected by forest fires and bush fires. Similarly, there is no adequate study of long-term data from ground and satellite-based estimation of fire foci in NEB. The objectives of this study are: (i) to evaluate the spatiotemporal estimation of fires in NEB biomes via environmental satellites during the long term over 1998–2018, and (ii) to characterize the environmental degradation in the NEB biomes via orbital products during 1998–2018, obtained from the Burn Database (BDQueimadas) for 1794 municipalities. The spatiotemporal variation is estimated statistically (descriptive, exploratory and multivariate statistics) from the Normalized Difference

Vegetation Index (NDVI), Enhanced Vegetation Index (EVI) and Standardized Precipitation Index (SPI) through the Climate Hazards Group InfraRed Precipitation Station (CHIRPS). Moreover, we identify 10 homogeneous groups of fire foci (G1–G10) with a total variance of 76.5%. The G1 group is the most extended group, along with the G2 group, the exception being the G3 group. Similarly, the G4–G10 groups have a high percentage of hotspots, with more values in the municipality of Grajaú, which belongs to the agricultural consortium. The gradient of fire foci from the coast to the interior of the NEB is directly associated with land use/land cover (LULC) changes, where the sparse vegetation category and areas without vegetation are mainly involved. The Caatinga and Cerrado biomes lose vegetation, unlike the Amazon and Atlantic Forest biomes. The fires detected in the Cerrado and Atlantic Forest biomes are the result of agricultural consortia. Additionally, the two periods 2003–2006 and 2013–2018 show periods of severe and prolonged drought due to the action of El Niño.

## 1. Introduction

Forest fires are a global natural disaster with a greater impact on forest ecosystem carbon cycling, and they are due to global warming, the annual increase in the amount of combustible materials and difficulties in controlling fire sources [1–3]. The climate and weather conditions are the dominant drivers of forest fires. Wu et al. [4] presented that global climate change can affect the frequency, intensity and the length of the wildfire season. Similarly, Li et al. [5] evaluated the climate change impact on future wildfire risk on the basis of Global Climate Models (GCMs) and suggested that climate change will increase the wildfire risk across the United States, particularly in the South Central region. However, the authors reported considerable variations across the future climate scenarios projected by the GCMs under the different Representative Concentration Pathway (RCP) scenarios proposed by Intergovernmental Panel on Climate Change (IPCC) Reports. The meteorological anomalies of surface temperature, surface pressure, precipitation, cloud water content, surface horizontal winds and 500 hPa vertical velocity were the main factors related to the devastating wildfires in California that occurred in October 2017 [5].

The wildfire risk and forest fire spread are also influenced by several other factors, such as topography, changes in LULC, distance from the road, source of ignition and moisture content of the fuel [6–13]. Moreover, the fire spread along the direction of the slope, elevation and topographic characteristics of the surface area are also important. For example, fires spread more quickly up-slope than down-slope. The up-slope fires accelerate the combustion process by the heat rise in front of the fire and dry the fuel faster up in the mountain more effectively [10–13]. Gheshlaghi [14] developed a fire risk map from slope, aspect, altitude, land cover, NDVI, yearly rainfall, temperature, distance to settlements and distance to roads in a Geographic Information System (GIS) based on analytical techniques. Furthermore, Salavati et al. [13] assessed fire risk potential in the city of Sanandaj in Western Iran using a statistical approach. They considered the local wildfire risk, including altitude, slope percentage, slope direction, distance from the road, distance from the river, LULC, average annual rainfall and average annual temperature as main factors. The above findings can assist decision-makers in taking appropriate precautions to prevent forest and rangeland fires and/or to minimize the fire damages.

Several approaches have been used to understand the forest fire propagation and wildfire risk to improve the fire control [15–17]. Cellular Automata (CA) have been used for a long time to model the complicated mechanism of fire spread [18]. Such simulations are driven by the Rate of Fire Spread (ROS), which is difficult to assess, hindering its implementation in the forest fire management system so far. Li et al. [18] also proposed two modified ROS models in order to improve the risk management and effectively implement fire suppression policies. They used a normal Long Short-Term Memory (LSTM)-based

speed model with a one-dimensional matrix consisting of wind speed and ROS as inputs. As an important conclusion from the study, the authors indicated that the process of forest fire spread is very complex, where the ROS was influenced by many factors, and indicated the need for more studies on this issue.

Forest fires annually destroy millions of hectares of productive land worldwide [19,20]. Brazil is among the countries that are the most affected by forest fires and burned cases [21,22]. Forest fires differ from those occurring in Brazil due to the extent of their effects, changes in LULC and use for deforestation [23,24]. It is worth noting that the use of fire is a cultural practice in Brazil, being applied in the management of agricultural crops, in the creation and maintenance of pastures for livestock and for cleaning urban waste [21,25]. Today, the impact of wildfires on the Earth's climate is a global concern due to the global emissions of water vapor ($H_2O$), carbon dioxide ($CO_2$), methane ($CH_4$), nitrogen dioxide ($N_2O$) and aerosols that are changing the Earth's radiative balance [26]. The aerosols reduce the transmission of solar energy to the Earth's surface, while greenhouse gases (GHGs) trap solar radiation [26,27]. Forest fire is a primary process to influence the composition and structure of the vegetation of the affected site and further exert a direct impact on biogeochemical cycles and the landscape [28,29].

In Brazil, forest fires are a concern among society and a governance problem, mainly due to the emission of GHGs that contribute to global warming [23,30]. GHG emissions via fires contribute to increased air pollution and worsening air quality in several metropolitan regions (MR) of Brazil [31,32]. Fires also contribute to the reduction of water in forests, affect human health and cause the intensification of extreme rainfall via increased condensation nuclei [33,34]. Since 1997, Brazil has been monitoring fire foci on the basis of the calculation and forecasting of the fire risk using environmental satellites from the Burn Database (BDQueimadas) developed by the Weather Forecast and Climate Studies Center (CPTEC)/Institute National Space Research Institute (INPE) [35]. BDQueimadas helps to prevent and minimize the environmental impacts caused by fires, especially in Environmental Preservation Areas (EPA), Conservation Units (CU) and Legal Reserves (LR) in the country [22,23,25,36]. Facing a growing number of fires and burnings, Brazil created the National Center for the Prevention and Fighting of Forest Fires (PREVFOGO) [37].

Previously, the spatiotemporal analysis of the fire foci in the NEB was evaluated via multivariate analysis (cluster analysis—CA) using the Ward method [21]. NEB was the only homogeneous group of fire foci in Brazil formed during 1998–2011, and this group showed a strong influence on multi-scale meteorological systems and economic activities, including livestock, agriculture and agropastoral activities [21,22]. However, the dynamics of the environmental degradation were not addressed for the fire foci in the biomes existing in the NEB (Atlantic Forest, Caatinga, Cerrado and Amazon). Therefore, characterizing the variability of fire foci in the NEB from space and ground-based products is fundamental for the implementation of new public policies and environmental management. Therefore, the objectives of this study are to first evaluate the space-temporality of the fire foci in the biomes within the NEB via environmental satellites, and secondly to characterize the environmental degradation in the NEB biomes via satellite data.

Section 2.2 of this paper contains detailed information on fire foci data obtained for the years 1998–2018 via BDQueimadas. Section 2.3 describes the detailed formulation of the multivariate analyses for the distribution and counting of fire foci divided into homogeneous groups. Section 2.4 shows the products obtained via remote sensing regarding precipitation and vegetation indices in order to evaluate the behavior of vegetation and associate it with fire foci, in search of confirmation of the relationship between LULC and fire foci. Similarly, Section 3 includes the results and information related to the distribution of groups of fire foci in a temporal, annual, monthly and spatial manner. Furthermore, the spatiotemporal distribution is estimated from the NDVI, Enhanced Vegetation Index (EVI), Standardized Precipitation Index (SPI) and precipitation. Section 4 presents a precise discussion on all the results and Section 5 refers to the conclusions of the research in this study.

## 2. Materials and Methods

### 2.1. Study Area

The NEB region has an area of approximately 1,558,196 km$^2$ and a population of 53,081,510 inhabitants [38]. The NEB consists of nine states, namely: Maranhão (MA), Piauí (PI), Ceará (CE), Rio Grande do Norte (RN), Paraíba (PB), Pernambuco (PE), Alagoas (AL), Sergipe (SE) and Bahia (BA) (Figure 1). The NEB has high inter-annual and intra-annual rainfall variability, with the thermal influence of the Pacific and tropical Atlantic oceans, which control and modulate years of drought and floods in the region [39–41].
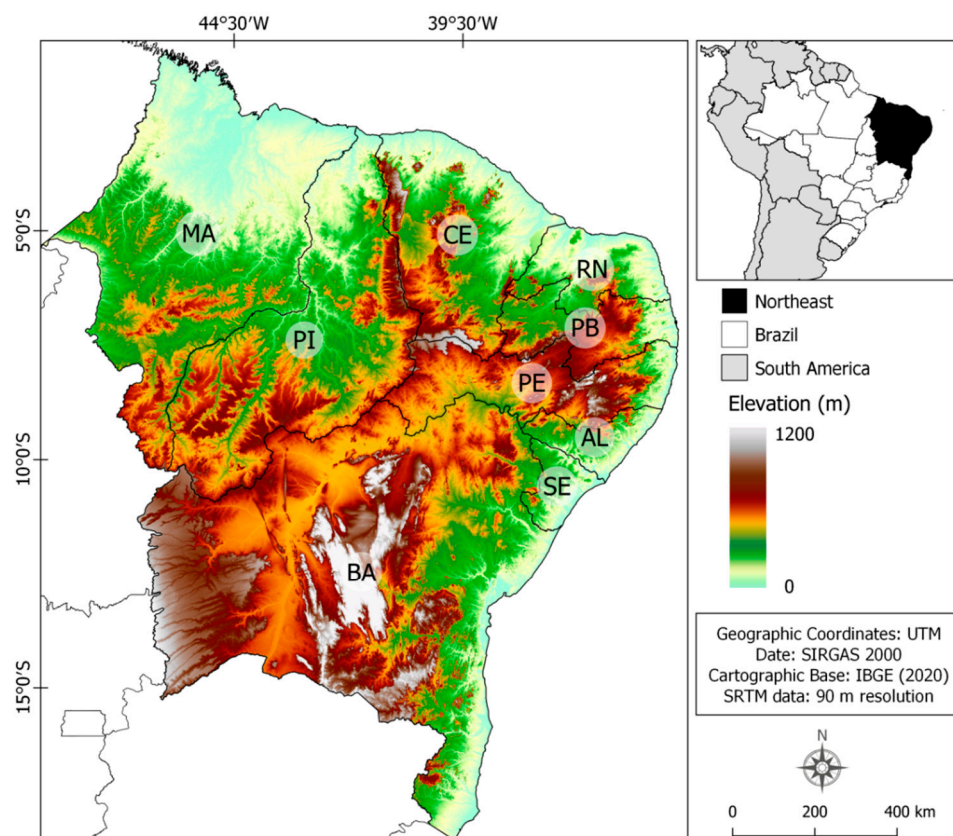


**Figure 1.** Location of the NEB in South America and the NEB highlighted with its elevation (m).

### 2.2. Fire Foci Data

Fire foci data were obtained from CPTEC/INPE via BDQueimadas [35]. Currently, CPTEC/INPE uses several environmental polar orbit and geostationary satellites in the composition of its observation network for the monitoring of fire foci in South America. The data are available in detail at the BDQueimadas website through the link http://pirandira.cptec.inpe.br/queimadas/, accessed on 20 January 2019. The long-term time series data of fire foci in 1794 municipalities in the NEB during 1998–2018 are analyzed in this study. The data were extracted by an algorithm in annual and monthly format.

### 2.3. Descriptive and Multivariate Analysis

For the characterization of homogeneous regions based on the records of fire foci of municipalities and states, CA was applied using the Euclidean distance measure [21,23], as shown in Equation (1):

$$d_{ab} = \left[ \frac{1}{N_{ab}} \sum_{j=1}^{N_{ab}} \left( X_{aj} - X_{bj} \right)^2 \right]^{1/2} \tag{1}$$

In the above equation, $X_{aj}$ is the $aj$th characteristic of the $a$th observation; $X_{bj}$ is the $j$th characteristic of the $b$th observation; $N_{ab}$ is the number of municipalities. Ward's method [21,23] was used in the study, according to Equation (2):

$$W = \sum_{k=1}^{K} \sum_{j=1}^{J} \sum_{i=1}^{N_k} \left( X_{ijk} - X_{\cdot jk} \right)^2 \tag{2}$$

In the above equation, $X_{ijk}$ is the value of the $j$th variable for the $i$th of the $N_k$ observations of the $K$ groups and $X_{\cdot jk}$ is the average value. The dot represents the average value of the sub-index.

After obtaining the constituted homogeneous groups, an exploratory analysis of the time series data was carried out, as well as the distribution of data on a monthly and annual scale for each group. This procedure allowed the detection of outliers, based on the expected average variation ranges of the data, and the identification of the temporal variability existing in the data. In descriptive statistics analysis part, the mean, the standard deviation, the frequency, the total and the maximum monthly values of fire foci were computed for each group, using the R programming environment (version 3.4-1).

*2.4. Remotely Sensed Data*

2.4.1. Vegetation Indices

The images acquired by the Moderate Resolution Imaging Spectroradiometer (MODIS) sensor were used for the temporal detection of the heat sockets on the biomes within in the NEB. The MODIS produces 16-day interval images at several spatial resolutions of the Vegetation Index (VI) products, values of the MOD13A1 and MYD13A1 products on the TERRA and AQUA satellites Didan [42]. Moreover, it is obtained for the years 2003–2006 and 2013–2018. The MOD13A1 and MYD13A1 products provide VI values at 500 m spatial resolution per pixel.

The two main vegetation layers, *EVI* and *NDVI*, are calculated from Equation (3) and Equation (4), respectively, to assess the attenuation of the effects of the soil. Furthermore, the effects of the Soil Adjusted Vegetation Index (SAVI) and atmosphere (adjusted by the Atmospherically Resistant Vegetation Index (ARVI)) are adjusted by the vegetation mapping [42].

$$EVI = g \frac{\rho_{IVP} - \rho_V}{\rho_{IVP} + (c_1 \times \rho_V) - (c_2 \times \rho_A) + L} \tag{3}$$

$$NDVI = \frac{\rho_{IVP} - \rho_V}{\rho_{IVP} + \rho_V} \tag{4}$$

where $\rho_{IVP}$, $\rho_V$ and $\rho_A$ are the reflectances in the spectral range of the near-infrared, red and blue, respectively. $g$ (gain factor) is 2.5, $c_1$ and $c_2$ are the correction coefficients for red (6) and blue (7.5) atmospheric effects, respectively, and $L$ is the correction factor for soil interference (1).

2.4.2. Precipitation

We used the monthly precipitation Climate Hazards Group InfraRed Precipitation with Stations (CHIRPS) product, the Climate Hazards Group (CHG) from the University of California at Santa Barbara (UCSB) (http://chg.geog.ucsb.edu/data/chirps/index.html, accessed on 20 January 2019) [43,44]. CHIRPS data are nearly real-time, updated, cover almost the entire globe (Earth only, 50° S–50° N) and incorporate a 0.05° resolution satellite (with 5.6 km) at different time scales (daily, monthly, decadal and pentadal). CHIRPS data are based on precipitation estimates from cold infrared (CCD) duration observations calibrated using the Multi-Satellite Precipitation Analysis by Tropical Rain Measurement Mission (TRMM/MSPA) with in situ data for the station from a variety of sources, including national and regional meteorological services [43,44]. In addition, the spatial resolution of CHIRPS is superior compared to other satellite-based global precipitation data sets.

2.4.3. Standardized Precipitation Index (SPI)

In order to identify the occurrence of drought and wet events, we used the SPI based on the CHIRPS precipitation product. The SPI formulation is based on the density and gamma probability function (Equation (5)) that is calculated every month, where $\alpha$ is the shape parameter ($\alpha > 0$), $\beta$ is the scale parameter ($\beta > 0$), which is determined using the maximum likelihood method, and $x$ is the amount of rainfall, which can vary according to $\alpha$ and $\beta$ [45].

$$g(\mathrm{x}) = \frac{1}{\beta^{\alpha}\Gamma(\alpha)}\ x^{\alpha-1}\ e^{-\frac{x}{\beta}} \tag{5}$$

where $\Gamma(\alpha)$ is the gamma function.

For the calculation of the SPI, time series of 12-month accumulations were generated and fitted to a two-parameter gamma distribution function. Finally, an equiprobability transformation from the cumulative density functions to the standard normal distribution with mean 0 and variance 1 was performed to obtain the SPI. Therefore, the SPI values are expressed in standard deviations, with positive or negative SPI values indicating greater or less than median precipitation, respectively. Three categories—dry, wet and normal—can be defined based on the SPI values, according to the methodology used by [45].

**3. Results**

*3.1. Descriptive and Multivariate Analysis*

3.1.1. Temporal

Cluster analysis highlighted the formation of 10 homogeneous sub-groups of fire foci (G1–G10) in the NEB, with a variance of 76.5% and a total number of 6,618,858 fire foci records in the studied period. High variability was observed between the groups in the absolute or relative number of fire foci, mean, standard deviation and maximum monthly values (Table 1). In these groups, G1 has the largest territorial extension, consisting of 1575 municipalities, and covers all biomes existing in the NEB, with a total of 2,130,317 foci (32% of the total events). Moreover, G2 is the second largest group, consisting of 144 municipalities, with a total of 1,459,133 foci (22% of the total number), and mainly covers Cerrado and Caatinga, with less coverage in the Amazon and the Atlantic forest. However, G3 is the smallest territorial extended group, formed of 37 municipalities, with a total of 815,221 foci (12.3% of the total of events), with coverage only in Cerrado. Groups 4 to 10 (G4–G10) consist of 38 municipalities, with a total of 2,214,187 fire foci, and hold the highest percentage (33.7% of the total of events), with coverage in Cerrado and the Amazon. In addition, the municipality of Grajaú (MA) presented the highest number of records (139,807 foci) and the maximum monthly number (18,812 foci) in relation to the other municipalities evaluated in the study. It is worth mentioning that the municipality of Grajaú is seriously affected by burnings in MA, most likely due its livestock and agriculture activities.

3.1.2. Annual

The annual analysis of fire foci is displayed in two distinct periods of the total study data, where period 1 (P1) denotes the years 2003–2006 and period 2 (P2) denotes 2013–2018 (Figure 2). Both periods were also characterized in the largest (G1 and G2) and smallest (G8 and G10) groups. According to the annual analysis, groups G3–G6 were all part of P2, whereas groups G7 and G9 did not have a defined period and displayed the highest number of outliers.

**Table 1.** Distribution of municipalities corresponding to the ten homogeneous groups of their total fire foci in the NEB, percentage (%), average and standard deviations and maximum monthly period during 1998–2018.

| Fire Foci Homogeneous Groups | Municipalities | Total (Foci)/ Percentual (%) | Average and Standard Deviation | Maximum Monthly |
|---|---|---|---|---|
| G1 | 1575 | 2,130,317/32.2% | (4.7 ± 6.5) | 32 |
| G2 | 144 | 1,459,133/22.0% | (40.6 ± 71.7) | 419 |
| G3 | 37 | 815,221/12.3% | (94.7 ± 212.0) | 1453 |
| G4 | 15 | 718,370/10.8% | (206.5 ± 448.6) | 2771 |
| G5 | 7 | 271,683/4.1% | (187.6 ± 419.3) | 2591 |
| G6 | 5 | 385,035/5.8% | (412.7 ± 827.7) | 6417 |
| G7 | 5 | 520,072/7.9% | (305.5 ± 594.1) | 8950 |
| G8 | 3 | 82,542/1.3% | (196.1 ± 923.0) | 7620 |
| G9 | 2 | 96,678/1.5% | (191.8 ± 931.3) | 12,212 |
| G10 | 1 | 139,807/2.1% | (554.8 ± 1803.3) | 18,812 |

Total Fire Foci—6,618,858 occurrences. Total Variance Explained—76.5%. The most representative groups: G1–G3 with 1736 municipalities; G4—Baixa Grande do Ribeiro, Buriti Bravo, Carolina, Cocos, Colinas, Correntina, Fernando Falcão, Jenipapo dos Vieiras, Loreto, Parnarama, Riachão, Ribeiro Gonçalves, Santa Filomena, São Raimundo das Mangabeiras e Tuntum; G5—Arame, Bom Jesus das Selvas, Buriticupu, Caxias, Codó, Matões e Santa Luzia; G6—Amarante do Maranhão, Cotegipe, Formosa do Rio Preto, Santa Rita de Cássia, São Desidério; G7—Alto do Parnaíba, Balsas, Barra do Corda, Mirador e Urucuí; G8—Bom Jardim, Centro Novo do Maranhão e Itinga do Maranhão; G9—Barra e Parnaguá; G10—Grajaú.

Despite G1 being the largest group in terms of territorial extension, it had a lower number of outliers (1999, 2006 and 2009) and total fire foci. The interquartile range in G1 was greater in P2 than in P1. The maximum values identified in this group did not exceed 30 foci per year (Figure 2a). G2 presented the highest record of outliers compared to all the other groups identified via CA, mainly during the years 1998–1999, 2002, 2006, 2009 and 2010–2014. Interestingly, these years were under the influence of the climate variability mode, El Niño—Southern Oscillation (ENSO), and its phases (El Niño—hot and La Niña—cold), respectively. The interquartile range was greater in the P2 period than in the P1 period also in G2. The maximum value identified in this group was greater than 300 foci per year (Figure 2b). Moreover, G2 presented a significant increase in the total number of fire foci in relation to G1. Within G3, a high portion of outliers were identified, with the exception of the years 2008, 2015 and 2017. G3 obtained maximum values of more than 300 foci annually in several years, including two years presenting values of approximately 1500 foci per year (Figure 2c), a threefold higher value in relation to G2. It is worth mentioning that between G3 and G10, there was a significant increase in the number of outliers within the studied years. Similar to G3, the G4 to G10 groups were the smallest in relation to the interquartile range, followed by an excessive number of outliers, with the exception of the years 2003, 2006, 2008 and 2014–2017. The maximum values varied between 3000 and 5000 foci per year (Figure 2d–h), the highest values recorded over the studied periods.
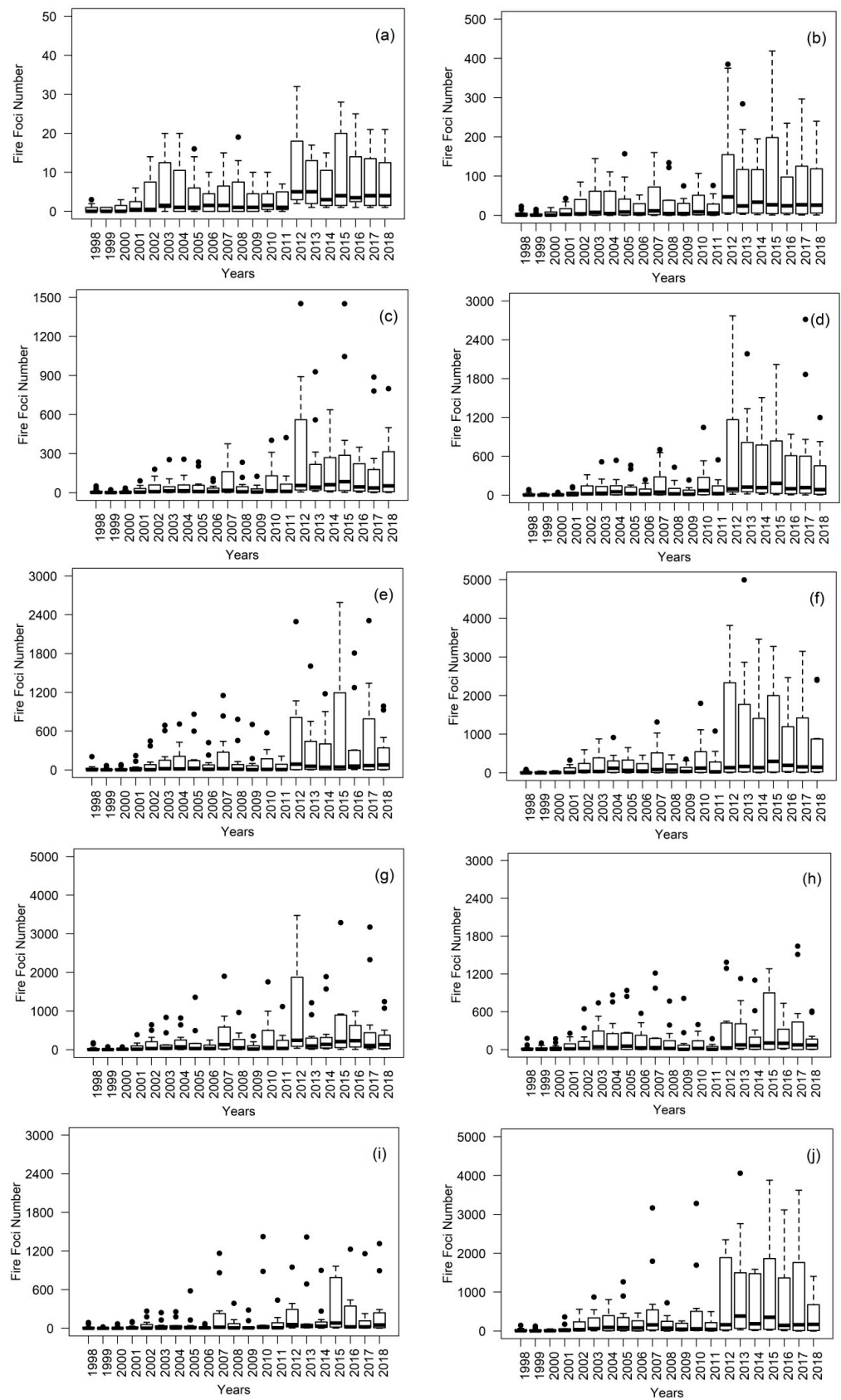
**Figure 2.** Annual boxplot of the fire foci of homogeneous groups (**a**) G1, (**b**) G2, (**c**) G3, (**d**) G4, (**e**) G5, (**f**) G6, (**g**) G7, (**h**) G8, (**i**) G9 and (**j**) G10 in the NEB in the period 1998–2018. • Annual boxplot of the 10 fire foci homogeneous groups.

### 3.1.3. Monthly

The analysis of the monthly fire foci in the NEB using a boxplot exhibited four distinct periods (P3–P6). These four periods refer to three, four, five and six consecutive months of the highest records, respectively (Figure 3). All periods mentioned deal with the spatiotemporal variability of precipitation in the NEB. P4 corresponded to groups G3, G6, G7 and G8, and P5 was related to groups G1, G4, G9 and G10, while the exceptions were G2 and G5, with associations with P3 and P6, respectively. In G1, the months showing high variability were August to December (P5), including an outlier in September. Comparable to the annual analysis, G1 had a lower number of outliers, mainly in January, February and April. Lastly, the monthly maximum values identified were greater than 30 foci per month (Figure 3a). In G2, the variable months were from July to December (P6), with outliers in almost each month, with the exceptions of January, February, August, September and October. Regarding the interquartile range, G2 was larger than G1, showing maximum values of more than 300 foci per month (Figure 3b). G3 presented a significant number of outliers, with October being the only exception, similar to the frequency of outliers in the annual scale. G3 had maximum records above 900 foci per month, even though it was lower than the consecutive months (P4) (Figure 3c). G4–G10 were basically formed by P4 and P5. These groups had an excessive number of outliers, excluding September and October. The maximum values varied between 3000 and 5000 foci per month (Figure 3d–i). One exception was the municipality of Grajaú (MA), with a maximum of 7500 foci per month (Figure 3j). Furthermore, the monthly outliers corresponded to monthly droughts or prolonged droughts in the NEB.

### 3.1.4. Spatial

The spatial distribution of the fire foci showed high variability along the NEB area, mainly on the coast, close to the Borborema Plateau (Figure 1), and within the existing biomes. It is worth noting the formation of a gradient of fire foci from the coast to the interior of the NEB, which is possibly associated with the changes in land use and occupation, and the variability of evapotranspiration (ET) (Figure 4). Group G1 (4.7 ± 6.5 foci) was concentrated close to the coastal region, followed by Agreste and Sertão in the NEB, mainly in the Amazon, Caatinga and Atlantic Forest biomes, with the exception of the Cerrado biome, with the lowest number of records (Figure 4a). Group G2 (40.6 ± 71.7 foci) was partly concentrated in the coastal region, over the states of MA and PI, and in the interior of the NEB, mainly in the Cerrado biome, with the exceptions of the Caatinga and Atlantic Forest biomes, with the smallest records (Figure 4b). Group G3 (94.7 ± 212.0 foci) was concentrated inside the NEB, including the states of BA, MA and PI, and fully inserted in the Cerrado biome, with the exceptions of the Amazon and the Caatinga biomes (Figure 4c). Finally, groups G4-G10 were similar to G2, with the concentration of fire foci in part of the coastal region of the states of MA and PI, followed by the northwest (NW) of BA, while the Amazon and Cerrado biomes were exclusive to these groups (Figure 4d).

### 3.2. *Land Use and Occupation via MODIS Product*
### 3.2.1. NDVI

Thematic maps of NDVI and EVI were generated based on the results obtained from the annual analysis (P1 and P2). The spatial variability of environmental degradation from the dense and abundant vegetation categories via NDVI was highlighted in the Amazon and Atlantic Forest biomes in P1, without significant variations in the (NW) portion, only in the Atlantic Forest biome (Figure 5). On the contrary, P2 exhibited a significant reduction in both biomes. The central region of the NEB showed the predominance of the barren land/built-up/rock categories at the beginning of P1 and along P2, while the sparse vegetation category increased significantly in P2, a period of severe drought in the NEB. Additionally, the category of water bodies remained unchanged regardless of the period evaluated. Comparatively, P1 and P2 showed a significant change in the NEB landscape, in the percentage of categories and in the coverage area.
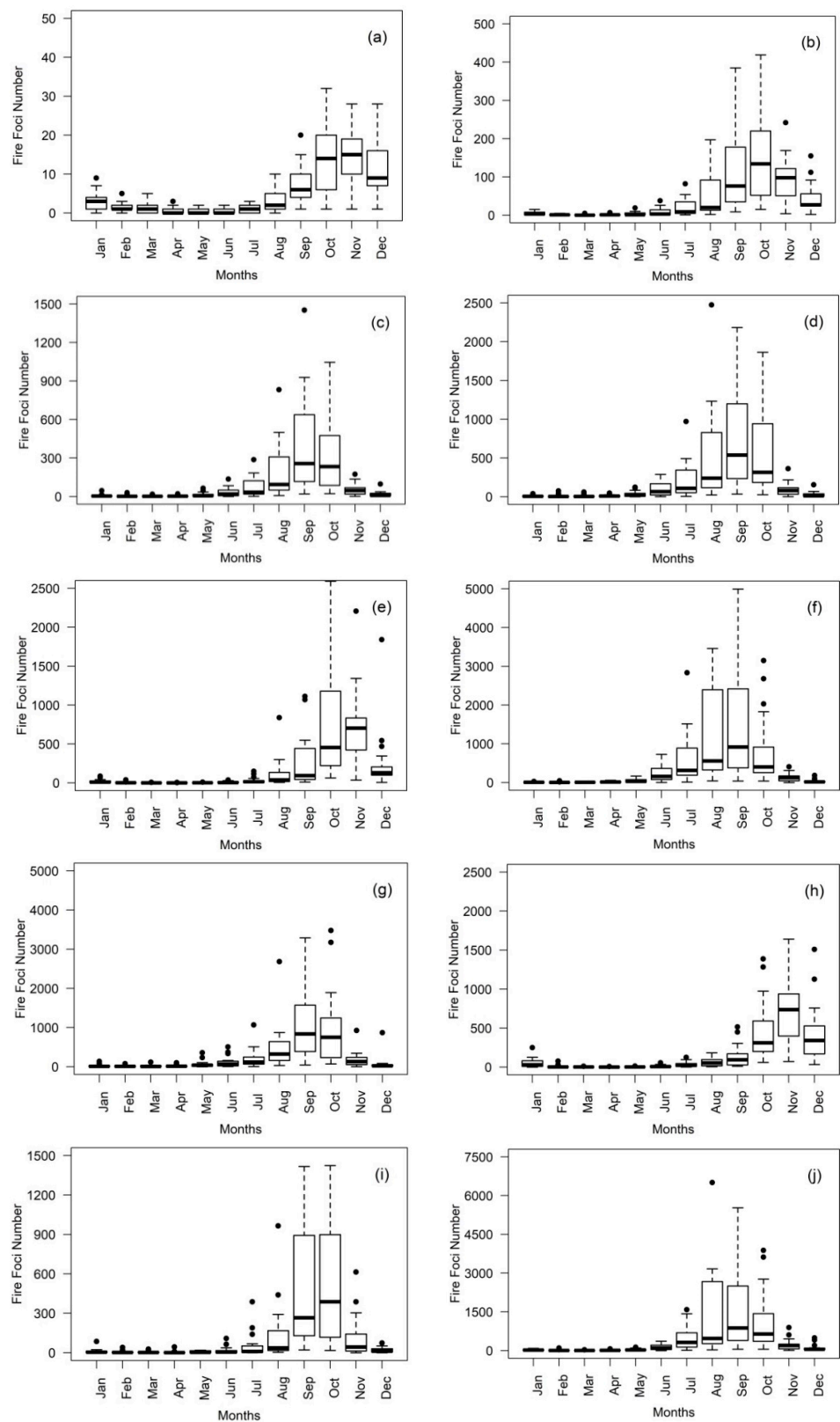
**Figure 3.** Monthly boxplot of the fire foci of homogeneous groups (**a**) G1, (**b**) G2, (**c**) G3, (**d**) G4, (**e**) G5, (**f**) G6, (**g**) G7, (**h**) G8, (**i**) G9 and (**j**) G10 in the NEB during 1998–2018. • Monthly boxplot of the 10 fire foci homogeneous groups.
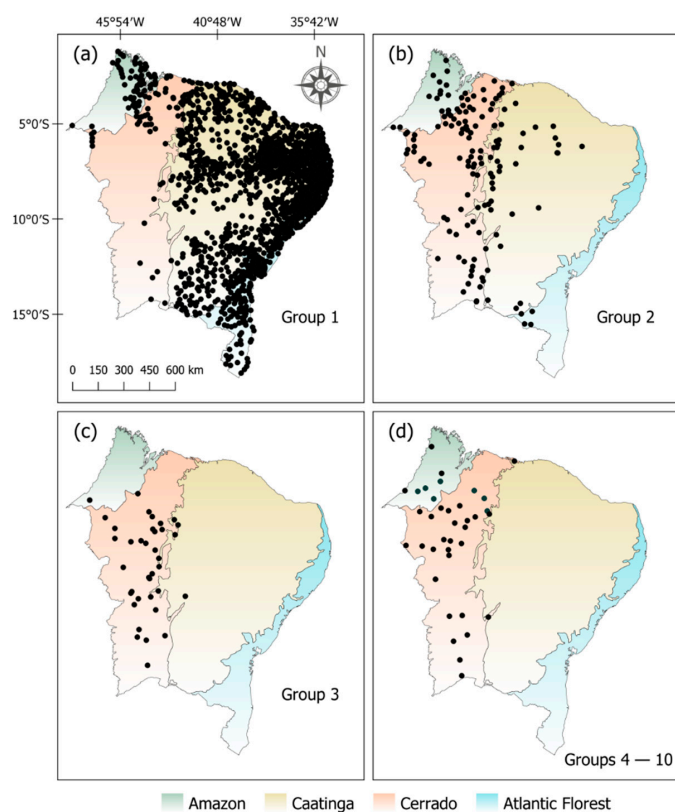
**Figure 4.** Spatial distribution of homogeneous groups of fire foci (**a**) G1, (**b**) G2, (**c**) G3 and (**d**) G4–G10 in the NEB in the period 1998–2018 and the respective Atlantic Forest, Cerrado, Caatinga and Amazon biomes.
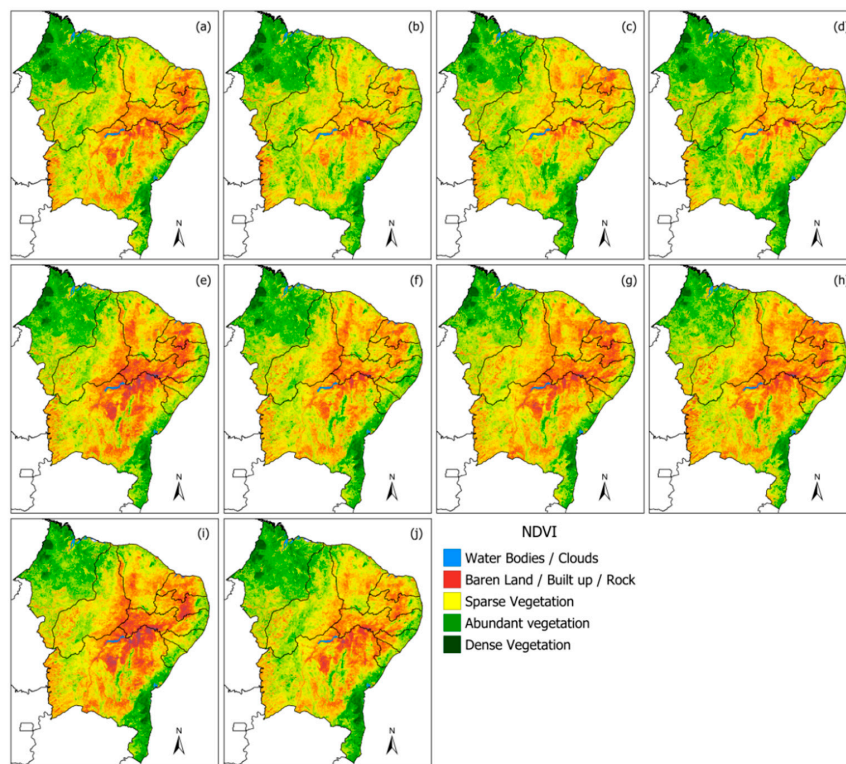


**Figure 5.** Spatial distribution of NDVI in (**a**) 2003, (**b**) 2004, (**c**) 2005, (**d**) 2006, (**e**) 2013, (**f**) 2014, (**g**) 2015, (**h**) 2016, (**i**) 2017 and (**j**) 2018 in the NEB.

In general, the greatest changes were observed in the Caatinga biome, being directly associated with the rainfall pattern, which alters the entire landscape. The vegetation of Caatinga has high sensitivity to changes in weather and climate; with this, any variation in the pluviometric regime causes a direct impact on the vegetation. In addition, human interference contributes to intense degradation, as shown in Figure 5.

### 3.2.2. EVI

Based on the EVI records, it was possible to identify changes in the vegetation of the biomes within the NEB, particularly in areas with an increase or decrease in vegetation (without vegetation). In the thematic maps, EVI values ranging from 0.3 to 0.5 indicate the presence of areas with vegetation, while areas of decreased or sparse vegetation and exposed soil have EVI values ranging from 0.0 to 0.3 (Figure 6). Significant accumulation of water, also known as water bodies, where the vegetation is typically poor, characterized by low EVI values (between 0.0 and 0.10), was observed throughout the NEB semiarid region. Low EVI values were observed mainly in the NE/SW areas of the NEB, which corresponds to the Caatinga and Cerrado biomes, respectively, with the intensified loss of vegetation over the years. However, the presence of areas with high vegetation density (>0.40) was observed in the Amazon and Atlantic Forest biomes.
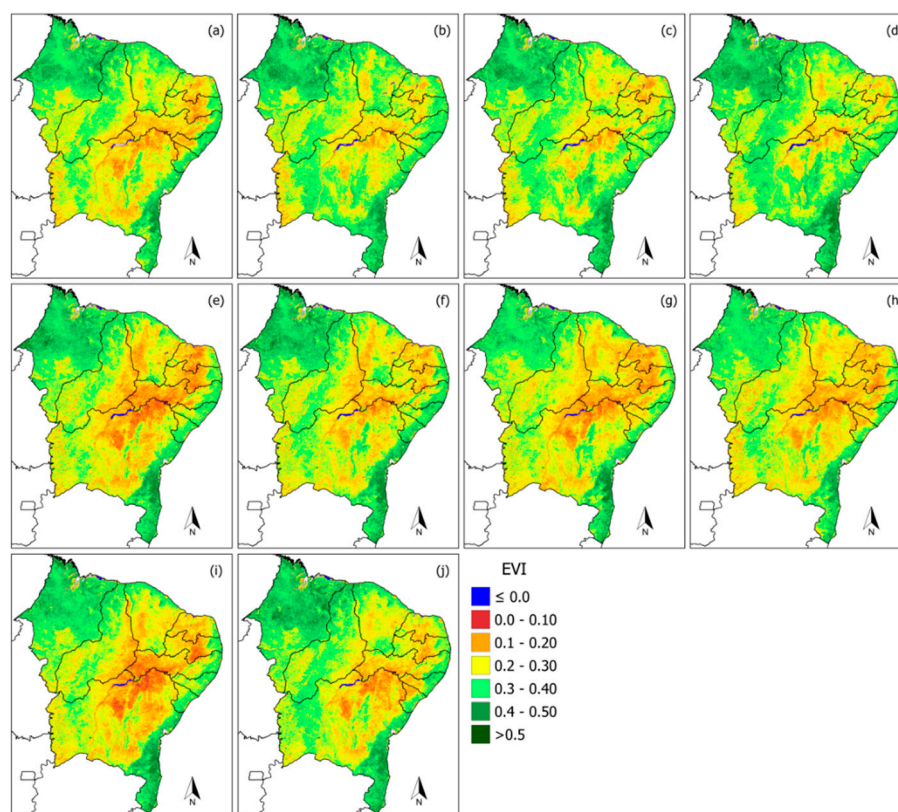


**Figure 6.** Spatial distribution of EVI (**a**) 2003, (**b**) 2004, (**c**) 2005, (**d**) 2006, (**e**) 2013, (**f**) 2014, (**g**) 2015, (**h**) 2016, (**i**) 2017 and (**j**) 2018 in the NEB.

### 3.3. Precipitation and SPI

#### 3.3.1. Precipitation (CHIRPS)

The CHIRPS annual rainfall archive showed high interannual variability in the NEB, highlighting the coastal region, with some sectors south, east and NW of the NEB, followed by the border regions of the Amazon and Cerrado biomes, with the highest total annual rainfall (between 1641 and 2200 mm). In the central and northern regions of the NEB, corresponding to the Caatinga and Atlantic Forest biomes, the total annual rainfall varied between 240 and 800 mm (Figure 7). Several of the studied years, located mainly in the

central and northern regions of the NEB, were dry—for example, 2003 and the period 2013–2017. It is known that the interannual rainfall variability in the NEB is highly conditioned by the ENOS climate variability mode, being intensified by the Pacific Decadal Oscillation (PDO) and by the influence of the Interhemispheric Gradient of the Atlantic Sea Surface Temperature (GITSMA).
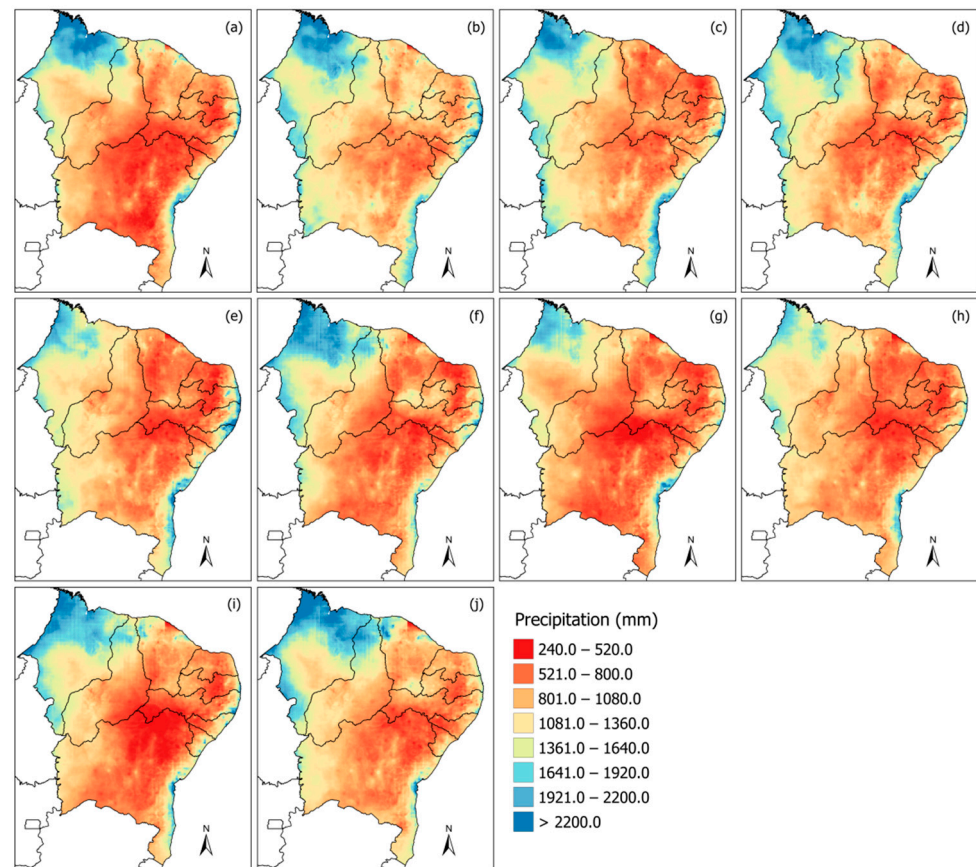


**Figure 7.** Spatial distribution of precipitation from CHIRPS (mm) for (**a**) 2003, (**b**) 2004, (**c**) 2005, (**d**) 2006, (**e**) 2013, (**f**) 2014, (**g**) 2015, (**h**) 2016, (**i**) 2017 and (**j**) 2018 in the NEB.

3.3.2. SPI

The largest records of extreme drought in NEB occurred in the years 2003 (neutral), 2015/2016 (El Niño) and 2017/2018 (La Niña) (Figure 8). Interestingly, some regions suffered from severe droughts—for instance, the areas composing the Cerrado and Caatinga biomes in the south of the NEB during 2003 (Figure 8a), all the NEB biomes during 2015 (Figure 8g), the Amazon, Atlantic Forest and Caatinga biomes on the coast and interior of the NEB during 2016 (Figure 8h), the Cerrado and Caatinga biomes located in the south of the NEB during 2017 (Figure 8i) and the NEB eastern coast, and mainly in the state of Alagoas, during 2018 (Figure 8j). The rainy years, in contrast, were identified during 2004–2006 (La Niña) and the year 2018, except the eastern coast.
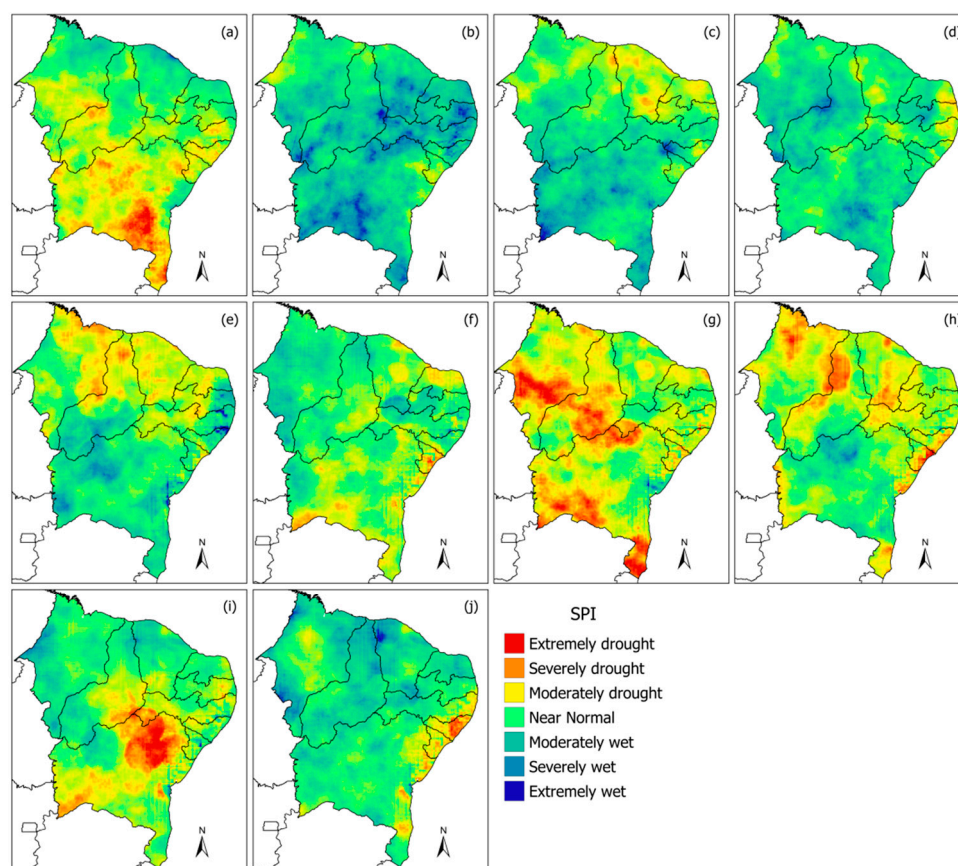
**Figure 8.** SPI spatial distribution for (**a**) 2003, (**b**) 2004, (**c**) 2005, (**d**) 2006, (**e**) 2013, (**f**) 2014, (**g**) 2015, (**h**) 2016, (**i**) 2017 and (**j**) 2018 in the NEB.

## 4. Discussion

According to the CA, the behavior of the fire foci could be categorized into 10 homogeneous groups (Table 1). It is worth mentioning that the CA technique has been applied in several studies of fire foci, with satisfactory results in Brazil [21,23] and worldwide [16,46]. The group G1 is located on the coast and in the interior of the NEB, and consists of the Caatinga, the Atlantic Forest and the Amazon biomes, emphasizing the lower occurrence in Cerrado. Group G1 also showed the highest population density, the lowest Human Development Indexes (HDI) [47,48] and the strongest LULC [49,50], being identified with the influence of socioeconomic data and LULC in other studies on fires around the world [2,4–6,10,11], since it is a region where large and rain-fed agriculture is concentrated [51,52]. The group G2 is located on a part of the north and inland NEB coast, corresponding to the Caatinga, the Cerrado and the Amazon biomes. Both G1 and G2 make up most of the NEB municipalities and are strongly influenced by the variability of ET, since the groups formed of ET are similar to groups of fire foci [53,54]. Rocha Júnior et al. [54] evaluated the influence of potential evapotranspiration (PET) on Northeastern Cerrado, and identified that the highest values occurred in the north of MA, with values ranging between 1250 and 2000 mm per year, while, in the Cerrado portion located in Bahia, the values oscillate between 600 and 1500 mm/year. The group G3 is fully inserted within Northeastern Cerrado, while the remaining groups, G4–G10, are fully inserted within the Amazon and Northeastern Cerrado biomes. The rainfall dynamics in groups G4–G10 are strongly conditioned by the biomes [55,56] and by the intense LULC in the border regions [57], mainly by the MATOPIBA agricultural consortium (acronym for the states: **MA**ranhão, **TO**cantins, **PI**auí and **BA**hia) [58,59].

The annual fire foci boxplot for the NEB identified two periods, P1 (2003–2006) and P2 (2013–2018) (Figure 2), both classified within the largest (G1 and G2) and the smallest

groups (G8 and G10) of fire foci. It is worth mentioning that both periods are influenced by the phases of ENSO and the variability of GITSMA, which influence rain dynamics in the NEB [39,45]. During the El Niño years, severe droughts occur, as discussed by Marengo et al. [60], while, during the La Niña years, large rainfall occurs [61,62], being duly characterized by the CHIRPS product (rainfall and SPI) (Figures 7 and 8). Due to the lack of consistent rainfall data in the NEB, the CHIRPS data were validated for the region, with satisfactory results [62]. It is known that the distribution of fire foci has a direct relationship with the inter-annual variability of rainfall in Brazil, and mainly in the NEB area [21,23,30], and this relationship is striking in the existing biomes in the NEB [22,56]. The monthly boxplot exhibited four distinct periods (P3, P4, P5 and P6—3, 4, 5 and 6 months, respectively) of the fire foci in the NEB (Figure 3). The abovementioned periods are influenced by the spatiotemporal variability of precipitation in the NEB [39–41,45]. Both periods defined in the NEB show the variability of the fire foci, where the largest (smallest) records of fire foci correspond to the dry season (transition and rainy seasons) [21,37,38], and it is therefore directly associated with the rainfall intra-annual variability and the multiscale meteorological systems that operate in the NEB [21–23,42]. In both the annual and the monthly scales, outliers that corresponded to severe or prolonged droughts in the NEB were identified [38,45,46].

The environmental degradation was identified by the NDVI and EVI vegetation indexes, widely used in the scientific literature [23,24,26,29,30]. The dense vegetation and the abundance categories, as identified via the NDVI, occurred in the Amazon and Atlantic Forest biomes in P1; however, in P2, a significant reduction in both biomes was recorded. Other studies [30,49,50] identified that drought events across the country were more severe and widespread between 2011 and 2017 based on the Integrated Drought Index (IDI), most likely owing to the increase in extreme drought events in P2 (El Niño and neutral years) [60–65], and the intensification of agricultural production of commodities (corn and soybeans) in the MATOPIBA (Amazon) consortia [58,59] and the SEALBA (acronym for the states: **SE**rgipe, **AL**agoas and **BA**hia) in the region of the coastal NEB [30,57]. In the central region of the NEB, a high proportion of the barren land, built-up and rock categories were registered at the beginning of P1 and along P2; however, the sparse vegetation increased significantly in P2. Notably, the central region, which includes the Caatinga biome, is characterized by a highly variable rainfall regime [53,55,56], and areas under a desertification process [47,50]. It is known that during extreme droughts, food security in the NEB semiarid region is under serious risk due to agricultural collapse, as highlighted recently by [40,64,65]. There are different statistical analyses for estimating fire foci throughout the world during long-term and short-term periods [62,66–68].

The limitations of the study are as follows: (i) it does not have a historical series of hotspots over 30 years and (ii) we do not have an ROS for the study region. The main recommendations for other studies are (i) to relate the hotspots to socioeconomic and environmental indicators, as well as to compare them with other drought indices existing in the literature, such as the PDSI and Reconnaissance Drought Index (RDI) among others; (ii) to characterize hotspot events with meteorological systems that can intensify fires in biomes—for example, Upper Tropospheric Cyclonic Vortices (UTCV) and the South Atlantic subtropical high (SASH).

## 5. Conclusions

Cluster analysis of the fire foci of biomes within in the NEB revealed 10 homogeneous subgroups. The different groups of fire foci presented both space and time variability, depending on the inter-annual and intra-seasonal rain regimes and alterations associated with land use and occupation. G1 covers all biomes present in the NEB, unlike G2, which mainly covers the Cerrado and the Caatinga biomes. The G3 group covered only Cerrado, and G4-G10 cover both the Cerrado and Amazon biomes. It is worth mentioning the fire foci gradient formation starting from the coast towards the inner areas of the NEB. Such a gradient is directly linked to changes in land use and occupation, which were identified

correspondingly by the vegetation indexes accounting for the sparse vegetation category (NDVI) and areas deprived of vegetation (EVI). This study made it possible to identify the loss of the vegetation over the years in the Caatinga and Cerrado biomes, unlike the significant increase in vegetation in the Amazon and Atlantic Forest biomes. The fire foci detected in the Cerrado biome are related to the expansion of agricultural consortia (MATOPIBA), while the fire foci detected in the Atlantic Forest biome and coastal areas are due to the SEALBA consortium.

## References

1. Hu, T.-X.; Zhao, B.-Q.; Li, F.; Dou, X.; Hu, H.-Q.; Sun, L. Effects of fire on soil respiration and its components in a Dahurian larch (*Larix gmelinii*) forest in northeast China: Implications for forest ecosystem carbon cycling. *Geoderma* **2021**, *402*, 115273. [CrossRef]
2. Valente, F.; Laurini, M. Spatio-temporal analysis of fire occurrence in Australia. *Stoch. Environ. Res. Risk Assess.* **2021**, *35*, 1759–1770. [CrossRef]
3. Wang, W.; Zhang, X.-L.; Dou, X.; Li, F. Effect of Moderate Fire Disturbance on Soil Phosphorus and Potassium of Dahurian Larch (*Larxi gmelinii*) Forest. *For. Eng.* **2020**, *36*, 10–18.
4. Wu, C.; Venevsky, S.; Sitch, S.; Mercado, L.M.; Huntingford, C.; Staver, A.C. Historical and future global burned area with changing climate and human demography. *One Earth* **2021**, *4*, 517–530. [CrossRef]
5. Li, A.X.; Wang, Y.; Yung, Y.L. Inducing factors and impacts of the October 2017 California wildfires. *Earth Space Sci.* **2019**, *6*, 1480–1488. [CrossRef]
6. Ganteaume, A.; Camia, A.; Jappiot, M.; San-Miguel-Ayanz, J.; Long-Fournel, M.; Lampin, C. A review of the main driving factors of forest fire ignition over Europe. *Environ. Manag.* **2013**, *51*, 651–662. [CrossRef] [PubMed]
7. Meng, Y.; Deng, Y.; Shi, P. Mapping forest wildfire risk of the world. In *World Atlas of Natural Disaster Risk*; Shi, P., Kasperson, R., Eds.; Springer: Berlin/Heidelberg, Germany, 2015; pp. 261–275.
8. Jaafari, A.; Gholami, D.M.; Zenner, E.K. A Bayesian modeling of wildfire probability in the Zagros Mountains, Iran. *Ecol. Inform.* **2017**, *39*, 32–44. [CrossRef]
9. Nami, M.; Jaafari, A.; Fallah, M.; Nabiuni, S. Spatial prediction of wildfire probability in the Hyrcanian ecoregion using evidential belief function model and GIS. *Int. J. Environ. Sci. Technol.* **2018**, *15*, 373–384. [CrossRef]
10. Juliev, M.; Mergili, M.; Mondal, I.; Nurtaev, B.; Pulatov, A.; Hübl, J. Comparative analysis of statistical methods for landslide susceptibility mapping in the Bostanlik District, Uzbekistan. *Sci. Total Environ.* **2019**, *653*, 801–814. [CrossRef] [PubMed]
11. Ma, W.; Feng, Z.; Cheng, Z.; Chen, S.; Wang, F. Identifying forest fire driving factors and related impacts in china using random forest algorithm. *Forests* **2020**, *11*, 507. [CrossRef]

12. Kayet, N.; Chakrabarty, A.; Pathak, K.; Sahoo, S.; Dutta, T.; Hatai, B.K. Comparative analysis of multi-criteria probabilistic FR and AHP models for forest fire risk (FFR) mapping in Melghat Tiger Reserve (MTR) forest. *J. For. Res.* **2020**, *31*, 565–579. [CrossRef]

13. Salavati, G.; Saniei, E.; Ghaderpour, E.; Hassan, Q.K. Wildfire Risk Forecasting Using Weights of Evidence and Statistical Index Models. *Sustainability* **2022**, *14*, 3881. [CrossRef]

14. Gheshlaghi, H.A. Using GIS to Develop a Model for Forest Fire Risk Mapping. *J. Indian Soc. Remote Sens.* **2019**, *47*, 1173–1185. [CrossRef]

15. Ljubomir, G.; Pamucar, D.; Drobnjak, S.; Pourghasemi, H.R. Modeling the spatial variability of forest fire susceptibility using geographical information systems and the analytical hierarchy process. In *Spatial Modeling in GIS and R for Earth and Environmental Sciences*; Pourghasemi, H.R., Gokceoglu, C., Eds.; Elsevier: Amsterdam, The Netherlands, 2019; pp. 337–369. [CrossRef]

16. Moayedi, H.; Mehrabi, M.; Bui, D.T.; Pradhan, B.; Foong, L.K. Fuzzy-metaheuristic ensembles for spatial assessment of forest fire susceptibility. *J. Environ. Manag.* **2020**, *260*, 109867. [CrossRef] [PubMed]

17. Sivrikaya, F.; Küçük, Ö. Modeling forest fire risk based on GIS-based analytical hierarchy process and statistical analysis in Mediterranean region. *Ecol. Inform.* **2022**, *68*, 101537. [CrossRef]

18. Li, X.; Zhang, M.; Zhang, S.; Liu, J.; Sun, S.; Hu, T.; Sun, L. Simulating Forest Fire Spread with Cellular Automation Driven by a LSTM Based Speed Model. *Fire* **2022**, *5*, 13. [CrossRef]

19. Jones, M.W.; Santín, C.; Van der Werf, G.R.; Doerr, S.H. Global fire emissions buffered by the production of pyrogenic carbon. *Nat. Geosci.* **2019**, *12*, 742–747. [CrossRef]

20. Park, M.; Worden, H.M.; Kinnison, D.E.; Gaubert, B.; Tilmes, S.; Emmons, L.K.; Boone, C.D. Fate of pollution emitted during the 2015 Indonesian Fire Season. *J. Geophys. Res. Atmos.* **2021**, *126*, e2020JD033474. [CrossRef]

21. Caúla, R.H.; Oliveira-Júnior, J.F.; Lyra, G.B.; Delgado, R.C.; Heilbron Filho, P.F.L. Overview of fire foci causes and locations in Brazil based on meteorological satellite data from 1998 to 2011. *Environ. Earth Sci.* **2015**, *74*, 1497–1508. [CrossRef]

22. Lima, G.S.; Torres, F.T.P.; Costa, A.G.; Félix, G.A.; Silva Júnior, M.R. Avaliação da Eficiência de Combate aos Incêndios Florestais em Unidades de Conservação Brasileiras. *Floresta* **2018**, *48*, 113–122. [CrossRef]

23. Silva Junior, C.A.; Teodoro, P.E.; Delgado, R.C.; Teodoro, L.P.R.; Lima, M.; Pantaleão, A.A.; Baio, F.H.R.; Azevedo, G.B.; Azevedo, G.T.O.S.; Capristo-Silva, G.F.; et al. Persistent fire foci in all biomes undermine the Paris Agreement in Brazil. *Sci. Rep.* **2020**, *10*, 16246. [CrossRef]

24. Lima, M.; Vale, J.C.E.; Costa, G.M.; Santos, R.C.; Correia Filho, W.L.F.; Gois, G.; Oliveira Júnior, J.F.; Teodoro, P.E.; Rossi, F.S.; Silva Junior, C.A. The Forests in the Indigenous Lands in Brazil in Peril. *Land Use Policy* **2020**, *90*, 1–3. [CrossRef]

25. Clemente, S.S.; Oliveira-Júnior, J.F.; Louzada, M.A.P. Focos de Calor na Mata Atlântica do Estado do Rio de Janeiro. *Rev. Bras. Meteorol.* **2017**, *32*, 669–677. [CrossRef]

26. Bowman, D.M.; Kolden, C.A.; Abatzoglou, J.T.; Johnston, F.H.; Van der Werf, G.R.; Flannigan, M. Vegetation fires in the Anthropocene. *Nat. Rev. Earth Environ.* **2020**, *1*, 500–515. [CrossRef]

27. Jiang, Y.; Yang, X.Q.; Liu, X.; Qian, Y.; Zhang, K.; Wang, M.; Lu, Z. Impacts of wildfire aerosols on global energy budget and climate: The role of climate feedbacks. *J. Clim.* **2020**, *33*, 3351–3366. [CrossRef]

28. Liu, J.; Qiu, L.; Wang, X.; Wei, X.; Gao, H.; Zhang, Y.; Cheng, J. Effects of wildfire and topography on soil nutrients in a semiarid restored grassland. *Plant Soil* **2018**, *428*, 123–136. [CrossRef]

29. Kumari, B.; Pandey, A.C. MODIS based forest fire hotspot analysis and its relationship with climatic variables. *Spat. Inf. Res.* **2020**, *28*, 87–99. [CrossRef]

30. Oliveira-Júnior, J.F.; Mendes, D.; Correia Filho, W.L.F.; Silva Junior, C.A.; Gois, G.; Jardim, A.M.R.F.; Silva, M.V.; Lyra, G.B.; Teodoro, P.E.; Pimentel, L.C.G.; et al. Fire Foci in South America: Impact and Causes, Fire Hazard and Future Scenarios. *J. S. Am. Earth Sci.* **2021**, *112*, 103623. [CrossRef]

31. Zeri, M.; Carvalho, V.S.B.; Cunha-Zeri, G.; Oliveira-Júnior, J.F.; Lyra, G.B.; Freitas, E.D. Assessment of the variability of pollutants concentration over the metropolitan area of São Paulo, Brazil, using the wavelet transform. *Atmos. Sci. Lett.* **2016**, *17*, 87–95. [CrossRef]

32. Squizzato, R.; Nogueira, T.; Martins, L.D.; Astolfo, R.; Bueno Machado, C.; de Fatima Andrade, M.; de Freitas, E.D. Beyond megacities: Tracking air pollution from urban areas and biomass burning in Brazil. *NPJ Clim. Atmos. Sci.* **2021**, *4*, 17. [CrossRef]

33. Hallema, D.W.; Sun, G.; Caldwell, P.V.; Norman, S.P.; Cohen, E.C.; Liu, Y.; Bladon, K.D.; McNulty, S.G. Burned forests impact water supplies. *Nat. Commun.* **2018**, *9*, 1–8. [CrossRef]

34. Reid, C.E.; Considine, E.M.; Watson, G.L.; Telesca, D.; Pfister, G.G.; Jerrett, M. Associations between respiratory health and ozone and fine particulate matter during a wildfire event. *Environ. Int.* **2019**, *129*, 291–298. [CrossRef] [PubMed]

35. Centro de Previsão do Tempo e Estudos Climáticos/Instituto Nacional de Pesquisas Espaciais (CPTEC/INPE). BDQueimadas—Banco de Dados Queimadas. Available online: http://www.cptec.inpe.br/queimadas/ (accessed on 20 January 2019).

36. Souza, T.C.O.; Delgado, R.C.; Magistrali, I.C.; Santos, G.L.; Carvalho, D.C.; Teodoro, P.E.; Silva Junior, C.A.; Caúla, R.H. Spectral trend of vegetation with rainfall in events of El Niño-Southern Oscillation for Atlantic Forest biome, Brazil. *Environ. Monit. Assess.* **2018**, *190*, 1–14. [CrossRef]

37. Instituto Brasileiro do Meio Ambiente e dos Recursos Naturais Renováveis (IBAMA). Centro Nacional de Prevenção e Combate aos Incêndios Florestais (Prevfogo). Available online: https://www.ibama.gov.br/prevfogo (accessed on 15 June 2019).

38. Instituto Brasileiro de Geografia e Estatística (IBGE). Área da Unidade Territorial: Área Territorial Brasileira. Rio de Janeiro. 2020. Available online: https://www.cidades.ibge.gov.br/brasil/al/panorama (accessed on 20 February 2020).

39. Lyra, G.B.; Oliveira-Júnior, J.F.; Zeri, M. Cluster analysis applied to the spatial and temporal variability of monthly rainfall in Alagoas state, Northeast of Brazil. *Int. J. Climatol.* **2014**, *34*, 3546–3558. [CrossRef]

40. Alvalá, R.C.S.; Cunha, A.P.M.A.; Brito, S.S.B.; Seluchi, M.E.; Marengo, J.A.; Moraes, O.L.L.; Carvalho, M.A. Drought monitoring in the Brazilian Semiarid region. *An. Acad. Bras. Ciênc.* **2017**, *89*, 1–15. [CrossRef]

41. Costa, M.S.; Oliveira-Júnior, J.F.; Santos, P.J.; Correia Filho, W.L.F.; Gois, G.; Blanco, C.J.C.; Teodoro, P.E.; Silva Junior, C.A.; Santiago, D.B.; Souza, E.O.; et al. Rainfall extremes and drought in Northeast Brazil and its relationship with El Niño-Southern Oscillation. *Int. J. Climatol.* **2020**, *41*, E2111–E2135. [CrossRef]

42. Didan, K. MOD13A1 MODIS/Terra Vegetation Indices 16-Day L3 Global 500 m SIN Grid V006 [Data Set]. NASA EOSDIS Land Processes DAAC. 2015. Available online: https://lpdaac.usgs.gov/products/mod13a1v006/ (accessed on 8 April 2021).

43. Funk, C.; Peterson, P.; Landsfeld, M.; Pedreros, D.; Verdin, J.; Shukla, S.; Husak, G.; Rowland, J.; Harrison, L.; Hoell, A.; et al. The climate hazards infrared precipitation with record for monitoring extremes. *Sci. Data* **2015**, *2*, 10–66. [CrossRef] [PubMed]

44. Funk, C.; Verdin, A.; Michaelsen, J.; Peterson, P.; Pedreros, D.; Husak, G. A global satellite-assisted precipitation climatology. *Earth Syst. Sci. Data* **2015**, *7*, 275–287. [CrossRef]

45. Lyra, G.B.; Oliveira-Júnior, J.F.; Gois, G.; Cunha-Zeri, G.; Zeri, M. Rainfall variability over Alagoas under the influences of SST anomalies. *Meteorol. Atmos. Phys.* **2017**, *129*, 157–171. [CrossRef]

46. Fuentes-Santos, I.; Marey-Pérez, M.F.; González-Manteiga, W. Forest fire spatial pattern analysis in Galicia (NW Spain). *J. Environ. Manag.* **2013**, *128*, 30–42. [CrossRef] [PubMed]

47. Pinto Vieira, R.M.S.; Sestini, M.F.; Tomasella, J.; Marchezini, V.; Pereira, G.R.; Barbosa, A.A.; Santos, F.C.; Rodriguez, D.A.; do Nascimento, F.R.; Santana, M.O.; et al. Characterizing spatio-temporal patterns of social vulnerability to droughts, degradation and desertification in the Brazilian Northeast. *Environ. Sustain. Indic.* **2020**, *5*, 100016. [CrossRef]

48. Oliveira-Júnior, J.F.; Correia Filho, W.L.F.; Alves, L.E.R.; Lyra, G.B.; Gois, G.; Silva Junior, C.A.; Santos, P.J.; Sobral, B.S. Fire Foci Dynamics and their relationship with socioenvironmental factors and meteorological systems in the state of Alagoas, Northeast Brazil. *Environ. Monit. Assess.* **2020**, *192*, 1–26. [CrossRef]

49. Pereira Silva, L.; Xavier, A.P.C.; Silva, R.M.; Guimarães Santos, C.A. Modeling land cover change based on an artificial neural network for a semiarid river basin in northeastern Brazil. *Glob. Ecol. Conserv.* **2020**, *21*, e00811. [CrossRef]

50. Jardim, A.M.R.F.; Araújo Júnior, G.N.; Silva, M.V.; Santos, A.; Silva, J.L.B.; Pandorfi, H.; Oliveira-Júnior, J.F.; Teixeira, A.H.C.; Teodoro, P.E.; Lima, J.L.M.P.; et al. Using Remote Sensing to Quantify the Joint Effects of Climate and Land Use/Land Cover Changes on the Caatinga Biome of Northeast Brazilian. *Remote Sens.* **2022**, *14*, 1911. [CrossRef]

51. CONAB. Séries Históricas de Produção de Grãos. 2018. Available online: http://www.conab.gov.br/conteudos.php?a=1252&t=2 (accessed on 20 March 2018).

52. IBGE. Sistema IBGE de Recuperação Automática. Territórios. 2021. Available online: https://sidra.ibge.gov.br/territorio (accessed on 9 April 2021).

53. Correia Filho, W.L.F.; Santos, T.V.; Santiago, D.B.; Oliveira-Júnior, J.F.; Amorim, R.F.C. Influence of meteorological variables on reference Evapotranspiration in the State of Alagoas, Brazil, based on multivariate analysis. *Model. Earth Syst. Environ.* **2021**, *7*, 2215–2224. [CrossRef]

54. Rocha Júnior, R.L.; Santos Silva, F.D.; Costa, R.L.; Gomes, H.B.; Gomes, H.B.; Silva, M.C.L.; Pinto, D.D.C.; Herdies, D.L.; Cabral Júnior, J.B.; Pita-Díaz, O. Mudança de Longo Prazo e Regionalização da Evapotranspiração de Referência no Nordeste Brasileiro. *Rev. Bras. Meteorol.* **2021**, *35*, 891–902. [CrossRef]

55. Fritzsons, E.; Mantovani, L.E.; Wrege, M.S. Os biomas e o clima das capitais do Brasil. *Rev. Bras. Geo. Fís.* **2017**, *10*, 1152–1160. [CrossRef]

56. Correia Filho, W.L.F.; Oliveira Júnior, J.F.; Santiago, D.B.; Terassi, P.M.B.; Teodoro, P.E.; Gois, G.; Blanco, C.J.C.; Souza, P.H.A.; Costa, M.; Santos, P.J. Rainfall variability in the Brazilian northeast biomes and their interactions with meteorological systems and ENSO via CHELSA product. *Big Earth Data* **2019**, *3*, 315–337. [CrossRef]

57. Silva Junior, C.A.; Costa, G.M.; Rossi, F.S.; Vale, J.C.E.; Lima, R.B.; Lima, M.; Oliveira-Júnior, J.F.; Teodoro, P.E.; Santos, R.C. Remote Sensing for Updating The Boundaries Between The Brazilian Cerrado-Amazonia Biomes. *Environ. Sci. Policy* **2019**, *101*, 383–392. [CrossRef]

58. Araújo, M.L.S.; Sano, E.E.; Santos, J.R.N.; Santos, J.S.; Brito Silva, F. Spatiotemporal dynamics of soybean crop in the Matopiba region, Brazil (1990–2015). *Land Use Policy* **2019**, *80*, 57–67. [CrossRef]

59. Reis, L.C.; Silva, C.M.S.E.; Bezerra, B.G. Analysis of Climate Extreme Indices in the MATOPIBA Region, Brazil. *Pure Appl. Geophys.* **2020**, *177*, 4457–4478. [CrossRef]

60. Marengo, J.A.; Alves, L.M.; Alvalá, R.C.S.; Cunha, A.P.; Brito, S.; Moraes, O.L.L. Climatic characteristics of the 2010–2016 drought in the semiarid Northeast Brazil region. *An. Acad. Bras. Ciênc.* **2018**, *90*, 1973–1985. [CrossRef]

61. Kogan, F.; Guo, W. Strong 2015–2016 El Niño and implication to global ecosystems from space data. *Int. J. Remote Sens.* **2016**, *30*, 161–178. [CrossRef]

62. Shah, M.; Abbas, A.; Ehsan, M.; Aiber, A.C.; Adhikari, B.; Tariq, M.A.; Ahmed, J.; Júnior, J.F.O.; Yan, J.; Morales, A.M.; et al. Ionospheric-Thermospheric Responses to the August 2018 Geomagnetic Storm over South America from Multiple Satellites. *IEEE J. Sel. Top. Appl. Earth Obs. Remote Sens.* **2022**, *15*, 261–269. [CrossRef]

63. Paredes-Trejo, F.J.; Barbosa, H.A.; Kumar, T.V.L. Validating CHIRPS-based satellite precipitation estimates in Northeast Brazil. *J. Arid Environ.* **2017**, *139*, 26–40. [CrossRef]

64.  Cunha, A.P.M.A.; Zeri, M.; Deusdará Leal, K.; Costa, L.; Cuartas, L.A.; Marengo, J.A.; Tomasella, J.; Vieira, R.M.; Barbosa, A.A.; Cunningham, C.; et al. Extreme Drought Events over Brazil from 2011 to 2019. *Atmosphere* **2019**, *10*, 642. [CrossRef]
65.  Marengo, J.A.; Cunha, A.P.M.A.; Nobre, C.A.; Ribeiro Neto, G.G.; Magalhaes, A.R.; Torres, R.R.; Sampaio, G.; Alexandre, F.; Alves, L.M.; Cuartas, L.A.; et al. Assessing drought in the drylands of northeast Brazil under regional warming exceeding 4 °C. *Nat. Hazards* **2020**, *103*, 2589–2611. [CrossRef]
66.  Shah, M.; Ehsan, M.; Abbas, A.; Ahmed, A.; Jamjareegulgarn, P. Possible Thermal Anomalies Associated With Global Terrestrial Earthquakes During 2000–2019 Based on MODIS-LST. *IEEE Geosci. Remote Sens. Lett.* **2022**, *19*, 1–5. [CrossRef]
67.  Shah, M.; Calabia, A.; Tariq, M.A.; Ahmed, J.; Ahmed, A. Possible ionosphere and atmosphere precursory analysis related to Mw > 6.0 earthquakes in Japan. *Remote Sens. Environ.* **2020**, *239*, 111620. [CrossRef]
68.  Shah, M.; Ahmed, A.; Ehsan, M.; Khan, M.; Tariq, M.A.; Calabia, A.; Rahman, Z. Total electron content anomalies associated with earthquakes occurred during 1998–2019. *Acta Astronaut.* **2020**, *175*, 268–276. [CrossRef]